

# 13

## Micro-pattern gaseous detectors

### 13.1 The micro-strip gas counter

The localization and rate limits of wire-based detectors were discussed in previous chapters. An innovative device named the micro-strip gas counter (MSGC) (Oed, 1988) appeared to fulfil the increasingly demanding requirements of particle physics experiments: improved position and multi-track resolution, and larger particle flux capability.

The MSGC structure consists of thin parallel metal strips, alternately narrow and wide, engraved on a thin insulating support, and connected respectively as anodes and cathodes; the detector is completed by an upper electrode delimiting the sensitive gas-filled drift gap. Using standard photolithographic technologies, a distance between strips, or pitch, of one hundred microns or below can be obtained, an order of magnitude improvement in granularity over wire chambers; Figure 13.1 is a close view of the anode ends in one of the first MSGCs, with 10  $\mu\text{m}$  wide anode strips at 200  $\mu\text{m}$  pitch, alternating with wider cathodes. The rear side of the support plate, or backplane, can also have a field-defining electrode that may be segmented to perform two-dimensional localization.

With appropriate potentials applied to the electrodes, electrons released in the drift gap move towards the strips and multiply in the high field region close to the anodes. In most cases, for convenience of readout, the anode strips are at ground potential, with the cathodes connected individually or in groups to the negative potential through high value protection resistors. Figure 13.2 shows the electric field in the vicinity of the strips, computed with anodes and backplane at equal potentials. All field lines from the drift volume terminate on the anodes, providing full electron collection efficiency; due, however, to the transverse dispersion of the avalanche during multiplication, a large fraction of the positive ions generated near the anode spreads into the field lines connecting to cathodes, and is quickly

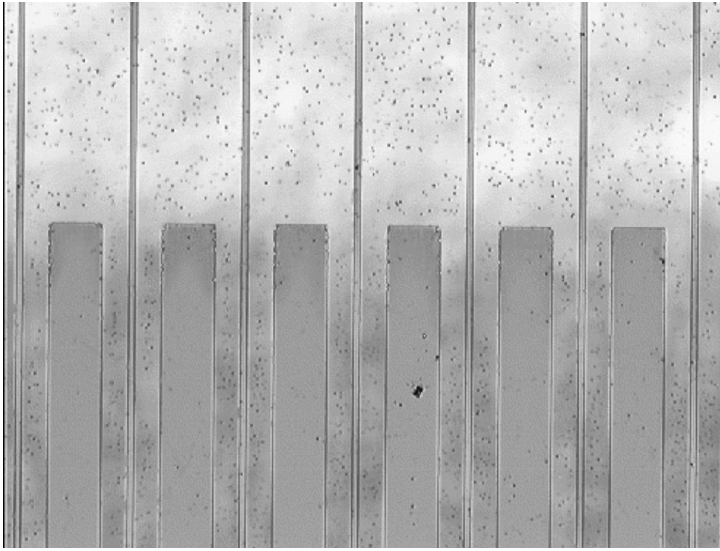


Figure 13.1 Close view of an MSGC plate, with narrow anodes alternating with wider cathode strips (Oed, 1988). By kind permission of Elsevier.

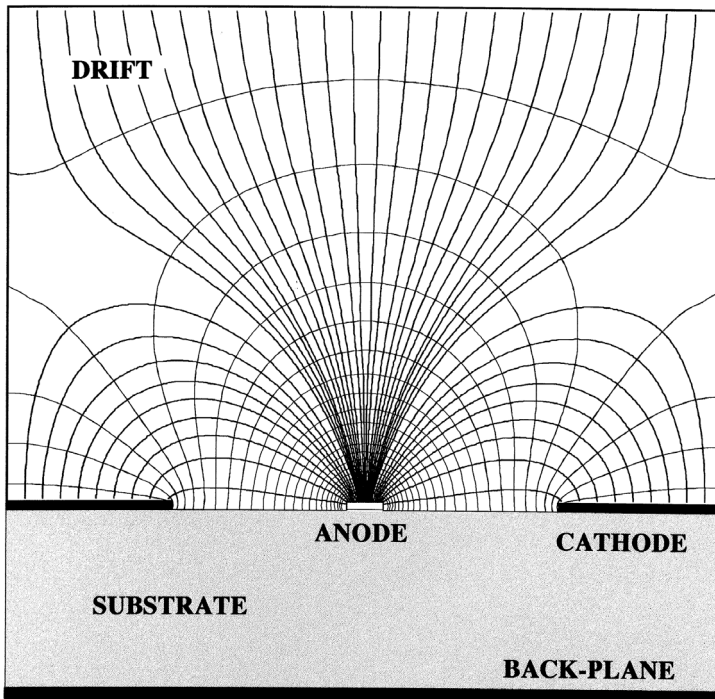


Figure 13.2 MSGC electric field in the vicinity of the strips.

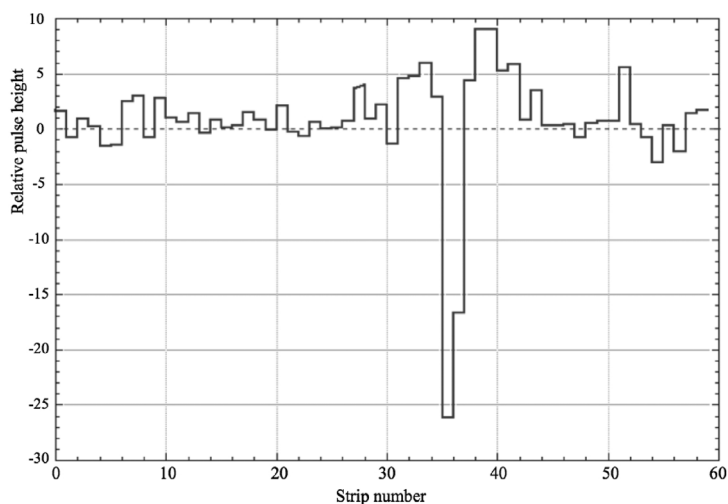


Figure 13.3 Anodic pulse height distribution for a charged particle track perpendicular to the detector. The strip pitch is 200  $\mu\text{m}$  (Bouclier *et al.*, 1995a). By kind permission of Elsevier.

collected; this substantially reduces the positive ion backflow in the drift gap, and results in much smaller field distortions as compared to wire-based devices.

At the occurrence of an avalanche, the fast electron collection and the retrograde motion of ions generate negative signals on the anodes; signals of opposite polarity are induced on the near cathodes, backplane and drift electrode. Due to stray capacitance between strips and to the drift electrode, a fraction of the signal induced on one set of strips is injected into the other, with amplitudes that depend on geometry, giving the typical charge distribution shown in Figure 13.3, sum of signals and noise (Bouclier *et al.*, 1995a). A calculation of the centre of gravity of the recorded distribution provides the position of localized avalanches; the width of the profile, 400  $\mu\text{m}$  in this example, determines the two-track resolution.

Microstrip detectors can be operated in a wide range of gases and pressures, and reach gains up to  $10^4$  with good proportionality. A compilation of measured gains in several gases at 1 bar, as a function of anode potential for a 200  $\mu\text{m}$  pitch, 10  $\mu\text{m}$  (100  $\mu\text{m}$ ) anode (cathode) strips width is given in Figure 13.4 (Beckers *et al.*, 1994). Particularly interesting choices are mixtures containing dimethyl ether (DME), thanks to its non-polymerizing properties (see Chapter 16). Detailed performance studies permitted one to optimize the geometry and operating conditions of the devices in view of their use for fast particle detection and localization (Florent *et al.*, 1993; Beckers *et al.*, 1994).

MSGC plates have been manufactured by photolithographic processing on a variety of supports and with several metals: chromium, aluminium, silver and gold.

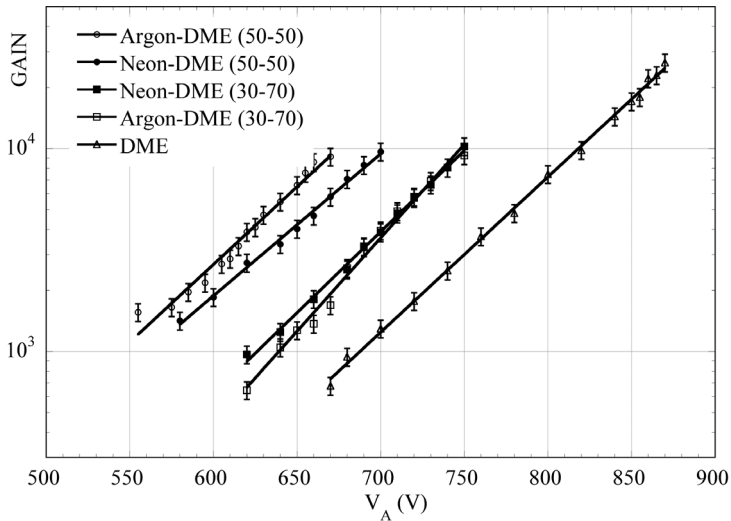


Figure 13.4 Gain as a function of voltage for several gas mixtures at STP (Beckers *et al.*, 1994). By kind permission of Elsevier.

The mechanical sturdiness of chromium is compensated by a higher resistivity, resulting in signal attenuation for long strips; gold plating is used to improve the performances and ease the connection to the readout electronics. The quality and uniformity of the artwork, and in particular smooth and defect-free edges of the strips, are paramount for a correct operation of the detectors. For a summary of manufacturing methods see Sauli and Sharma (1999).

Industrially produced up to sizes of  $30 \times 30 \text{ cm}^2$ , the rigid MSGC plates can be easily mounted as detector, inserted in a gas containment box or in framed assemblies, suitable for many applications. Figure 13.5 is a schematic view of the components of a light MSGC detector, used in extensive laboratory and beam tests (Bohm *et al.*, 1995). The active plate and a thin glass roof with an internal drift electrode are glued to an insulating frame with gas inlet and outlet; the readout electronics is connected on the anode strip side, and the high voltage provided to cathode strips and drift electrode through protection resistors. For fast beam tracking, the drift gap is usually around 3 mm thick; other values can be used for more efficient detection of soft X-rays.

Thanks to their high granularity and fast ion collection by neighbouring cathode strips, MSGCs were expected to tolerate high radiation fluxes. From the very beginning, however, various operating instabilities have been observed: time-dependent gain shifts, attributed to substrate polarization and charging up; permanent deterioration during sustained irradiation; tendency to discharge. The physical parameters used to manufacture and operate the detectors (substrate material, metal of the strips, type and purity of the gas mixture) play dominant

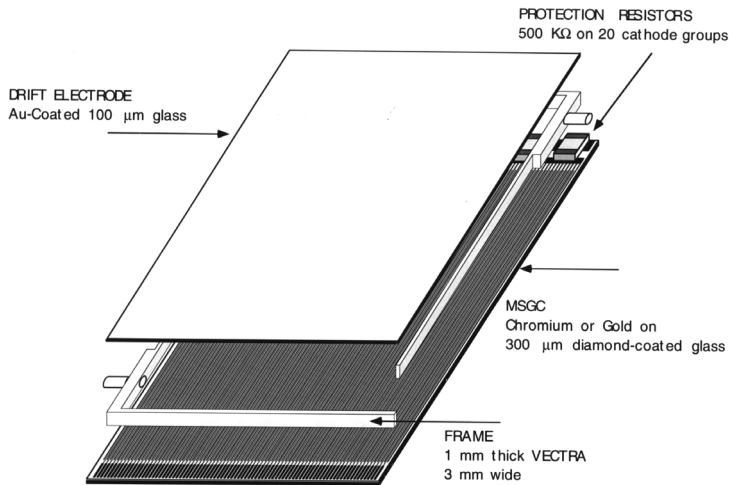


Figure 13.5 Schematics of a light MSGC assembly (Bohm *et al.*, 1995). By kind permission of Elsevier.

roles in determining the medium- and long-term stability (Bouclier *et al.*, 1992; Florent *et al.*, 1993). A research effort was undertaken to understand the MSGC operation, to improve their performance and lifetime, as well as reducing manufacturing costs, an essential goal in view of intensive use in large systems; at the peak of its activity, a collaboration for the development of MSGCs included more than 40 laboratories worldwide<sup>1</sup> (Sauli, 1998).

Use of supports with controlled resistivity permits one to neutralize the surface charge, and extends considerably the rate capability of the MSGC. Commercial, low resistivity glasses have been employed for this purpose, but appeared to rely on ionic conductivity, changing with time from the application of the electric field, an effect referred to as polarization of the dielectric. Better stability of performance has been obtained using electron-conducting substrates, originally developed for spark counters and named Pestov glass from the main developer (Frolov *et al.*, 1991); manufactured in a wide range of resistivity, they exhibit stable operation up to very high radiation fluxes, as shown in Figure 13.6, comparing the normalized gain as a function of rate, measured for soft X-rays, of MSGCs manufactured on commercial borosilicate glass 2 DESAG D-263, SHOTT speciality glass, Germany and on Pestov glass of two values of resistivity. For  $10^9$  Ohms cm, the proportional gain is unaffected up to a flux of a  $\text{MHz mm}^{-2}$  (Bouclier *et al.*, 1995b).

An alternative solution is to cover a standard glass with a thin resistive coating before metallization and photolithographic processing; a diamond-like layer, produced by carbon vapour deposition (CVD) and with a surface resistivity around

<sup>1</sup> CERN RD28, F. Sauli, spokesman (1993–1996).

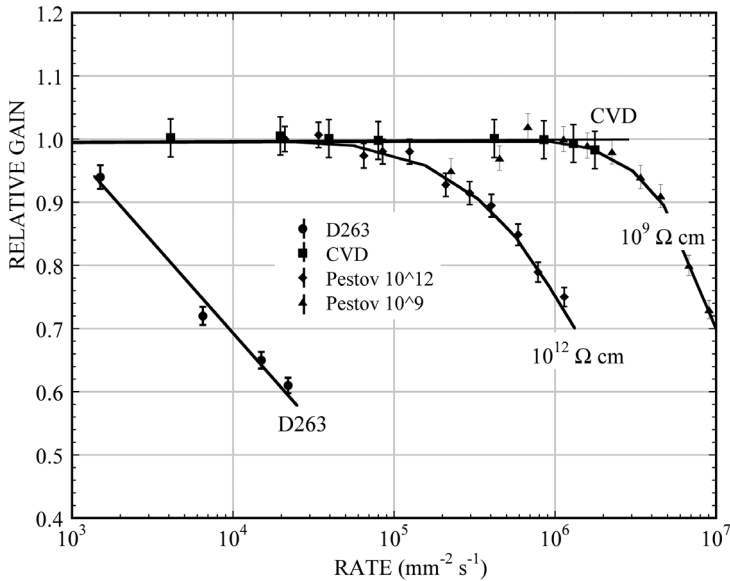


Figure 13.6 Rate dependence of normalized gain for different MSGC substrates (Bouclier *et al.*, 1995b). By kind permission of Elsevier.

$10^{14} \Omega/\text{square}$  provides equivalent or better rate capability, as shown in the figure (Bouclier *et al.*, 1996b). As the production of large plates of electron conducting glass turned out to be problematic, the CVD coating remains a good option, and has been used for detectors used in systematic measurements of performances (Barr *et al.*, 1996; Angelini *et al.*, 1996; Abbaneo *et al.*, 1998). As an example, Figure 13.7 shows the residual distribution recorded with a set of MSGCs in a minimum ionizing particle beam perpendicular to the detectors; the position accuracy is better than  $40 \mu\text{m rms}$  (Bouclier *et al.*, 1995a).

Introduced originally for applications as detectors in neutron spectrometry, MSGCs are successfully used in this field, using  $^3\text{He}$  as sensitive gas filling or internal thin-foil converters. A large one-dimensional neutron diffractometer making use of 48 MSGC plates in a semi-cylindrical array, four metres long, shown in Figure 13.8, has been operating for many years at Grenoble's Institute Laue Langevin (ILL), despite some observed deterioration of the anode strips (Clergeau *et al.*, 2001; Hansen *et al.*, 2008).

Two-dimensional localization can be performed with a segmented backplane readout, or various schemes of pad rows replacing the cathode strips on the active side of the plates, see for example Vellettaz *et al.* (2004); Masaoka *et al.* (2003); Takahashi *et al.* (2004); Fujita *et al.* (2007); Bateman *et al.* (2010); Bateman *et al.* (2012). An overview and comparison of neutron detectors is given in Oed (2004) and Buffet *et al.* (2005).

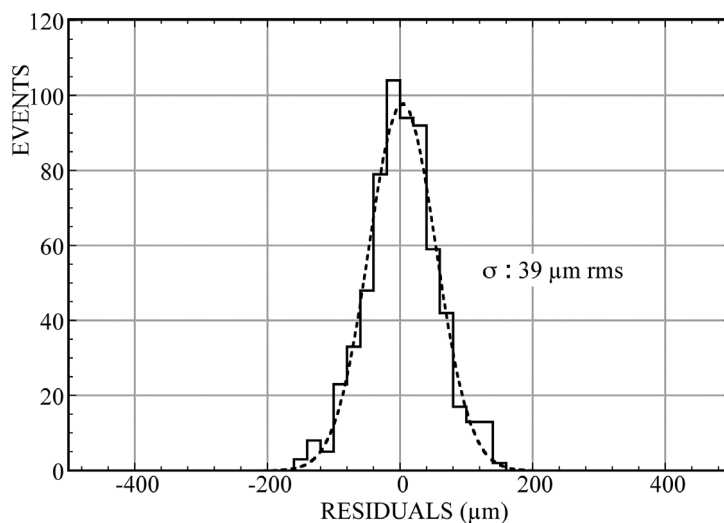


Figure 13.7 MSGC space accuracy for minimum ionizing particles (Bouclier *et al.*, 1995a). By kind permission of Elsevier.

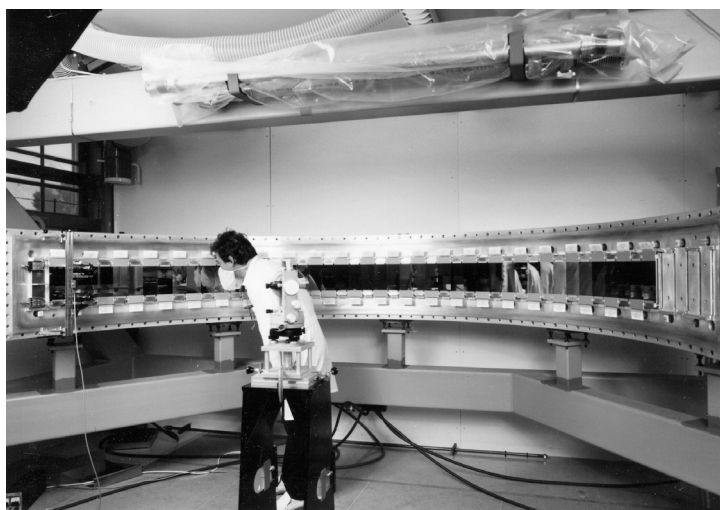


Figure 13.8 MSGC array for the ILL neutron diffractometer (Clergeau *et al.*, 2001). By kind permission of Elsevier.

The use of MSGCs, requiring a large number of readout channels, has been facilitated by the coincidental compatibility with the performances of circuits mass-produced for silicon strip detectors: indeed, the smaller ionization signal is compensated by the gain of the gaseous devices. Several particle physics experiments have been designed to use large arrays of MSGCs (Angelini *et al.*, 1995; Zeuner, 2000; Ackerstaff *et al.*, 1998). Disappointingly, and despite large

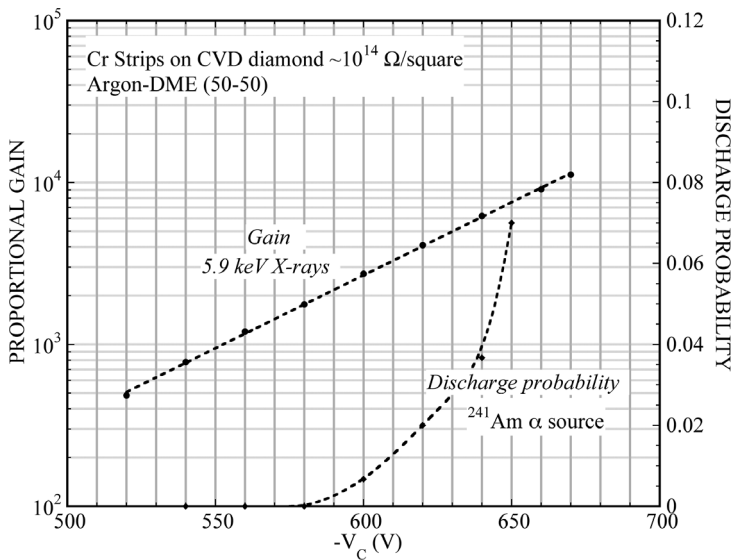


Figure 13.9 MSGC gain measured for soft X-rays, and discharge probability on exposure to  $\alpha$  particles (Bressan *et al.*, 1999a). By kind permission of Elsevier.

development efforts, the devices appeared prone to fast degradation and discharges when operated at the gains needed for detection of minimum ionizing particles, often causing irreversible damage to the fragile electrodes (Bouclier *et al.*, 1995c). A common observation has been that detectors that perform well in the laboratory under very high fluxes of soft X-rays experience instabilities and discharge-related damage when exposed to charged particle beams (Schmidt, 1998; Barr *et al.*, 1998). Indeed, albeit with small probability, ionization densities largely exceeding the normal can be deposited by interactions with the detector gas or materials of neutrons, nuclear fragments or electromagnetic showers; a neutron-produced  $\sim$ MeV proton releases in the gas three orders of magnitude more charge than a minimum ionizing track, exceeding the Raether limit discussed in Section 8.8 and leading to a discharge.

Since beam conditions are difficult to reproduce, a standard test for defining the threshold of appearance of discharges has been introduced, exposing the detectors to heavily ionizing sources; in a 3 mm sensitive gap, the average number of ionization electrons released by  $\sim$ MeV  $\alpha$  particles is around 5000. Figure 13.9 is an example of the gain measured with a soft X-ray source, and of the discharge probability on exposure to  $\alpha$  particles as a function of voltage<sup>2</sup> (Bressan, A. *et al.* (1999a)). Capable of reaching gains up to  $10^4$  in a benign environment, when

<sup>2</sup> The definition of discharge probability is somewhat arbitrary, as it depends on the source rate and the observation time. In view of its rapid exponential growth, however, it helps in defining a threshold voltage for breakdown.

exposed to highly ionizing radiation the onset of discharges limits the operation to gains below those needed for the detection of fast particles (around 5000 using standard available electronics).

A convenient  $\alpha$ -particle source is  $^{220}\text{Rn}$ , introduced in the chamber by inserting a natural thorium cartridge in the gas flow. Many innovative MPGD detectors, described in the following sections, have been systematically tested for resilience to discharges using this method, with comparable outcomes, a demonstration of the fundamental nature of the Raether limit (Bressan *et al.*, 1999a). A noticeable exception is observed by cascading several elements of amplification, each operated at reduced gain, with the use of multiple gas electron multiplier electrodes (GEM), discussed in Section 13.4. A GEM pre-amplifier electrode, added to the MSGC detector in the HERA-B experiment, permitted one to solve the discharge problem and operate the tracker for several years (Schmidt, 1998).

Aside from manufacturing defects, a source of discharges even in the absence of radiation has been identified in a process related to the double amplification discussed in Section 8.8 for wire counters. The electric field near the edges of the cathode strips can be high enough to impart a pre-amplification to ionization electrons released in their proximity, or by spontaneous field emission. A calculation of avalanche multiplication for electrons released in the vicinity of the cathode edges provides the equal-gain lines shown in Figure 13.10 (Beckers *et al.*, 1994); for a normal anodic gain around 2000, electrons released near the cathode edge are pre-amplified and experience a much larger total gain, easily leading to charge densities satisfying the Raether condition and provoking a discharge.

Coating the cathode strip edges with a thin layer of polyimide insulator, using a technique named advanced passivation, prevents or delays the spontaneous field emission at the cost of an increased complexity of manufacturing (Bellazzini *et al.*, 1998b).

Due to the small surface of the anodes MSGCs are particularly sensitive to the presence of thin insulating layers, as those created by gas polymerization or pollutants; great care in the gas purity and choice of construction materials is needed to prevent a fast deterioration (Bouclier *et al.*, 1994b). The subject of MSGC ageing will be discussed in detail in Chapter 16.

### 13.2 Novel micro-pattern devices

The problems encountered with the MSGCs spawned the development of alternative structures, collectively named micro-pattern gas detectors (MPGDs), capable of achieving comparable performances but more resistant to radiation and damages: micro-gap, micro-wire, micro-dot, field gradient lattice, 'compteur à trous' and others. For an overview of these devices and related references see Sauli and Sharma (1999).

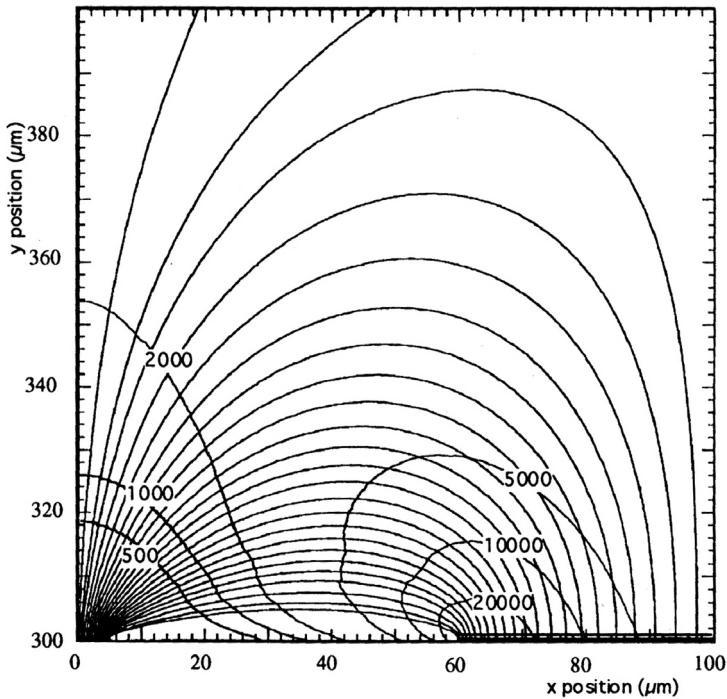


Figure 13.10 Computed equal gain lines in an MSGC. Charge pre-amplification can occur for electrons released in the vicinity of the cathode strip edges (Beckers *et al.*, 1994). By kind permission of Elsevier.

The technology of combining photolithography and thin-layer polyimide depositions, used to coat the cathode edges as described in the previous section, led to the development of structures designed to improve the insulation between anode and cathode strips, as the micro-gap (Angelini *et al.*, 1993) and the micro-groove chambers (Bellazzini *et al.*, 1998a), shown in Figure 13.11.

As many of the gain instabilities and discharge problems encountered in MPGDs are related to the presence of insulators, attempts have been made to build structures almost substrate-free: successive steps of photolithographic metal engraving and polymer wet etching result in devices with the insulator reduced to narrow pillars or bridges between metal strips, minimizing charging-up processes. Examples are the micro-wire chamber (Adeva *et al.*, 1999) and the field gradient lattice detector (FGLD) (Dick *et al.*, 2004), shown in Figure 13.12.

Alternative structures have been developed by exploiting the refined technologies used for solid-state circuit manufacturing on silicon supports. The micro-dot, Figure 13.13 left (Biagi and Jones, 1995), is a matrix of planar proportional counters, each consisting of a central round electrode (the anode) surrounded by one or more concentric electrodes; with suitable potentials applied to the

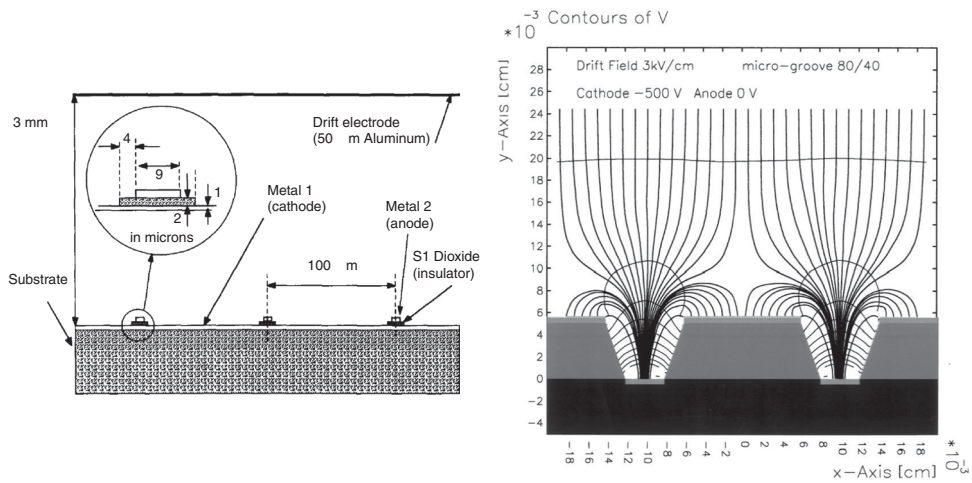


Figure 13.11 Schematics of the microgap, left (Angelini *et al.*, 1993) and micro-groove chambers, right (Bellazzini *et al.*, 1998a). By kind permission of Elsevier.

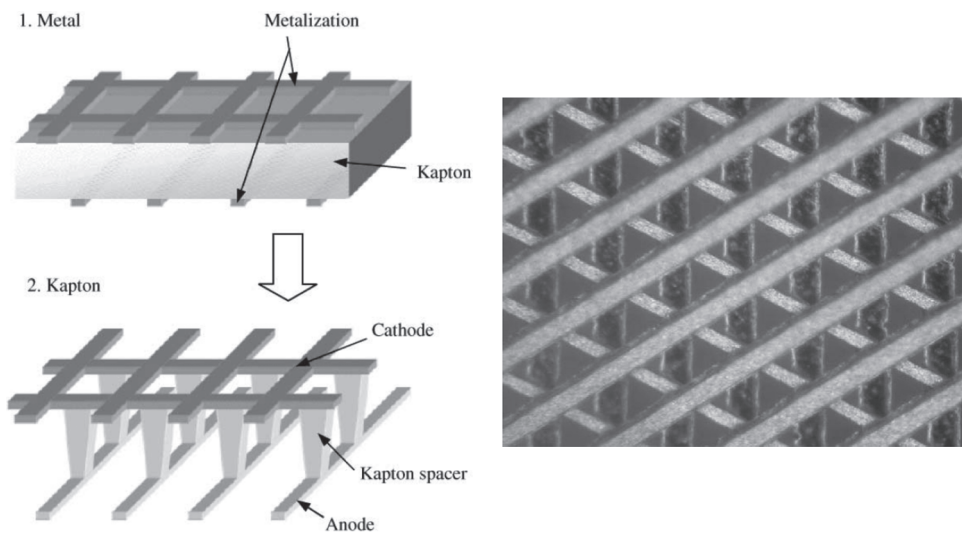


Figure 13.12 Schematics of the micro-wire chamber, left (Adeva *et al.*, 2001) and view of the FGLD, right (Dick *et al.*, 2004). By kind permission of Elsevier.

electrodes, each dot acts as an individual proportional counter, read out individually or interconnected in lines. The micro-pin array (MIPA), right, is a three-dimensional extension of the same structure, with metal points acting as anodes (Rehak *et al.*, 2000).

Similar in concept to the previous devices, but on a coarser scale, the micro-pixel chamber ( $\mu$ PIC), Figure 13.14, (Ochi *et al.*, 2002), features a matrix of

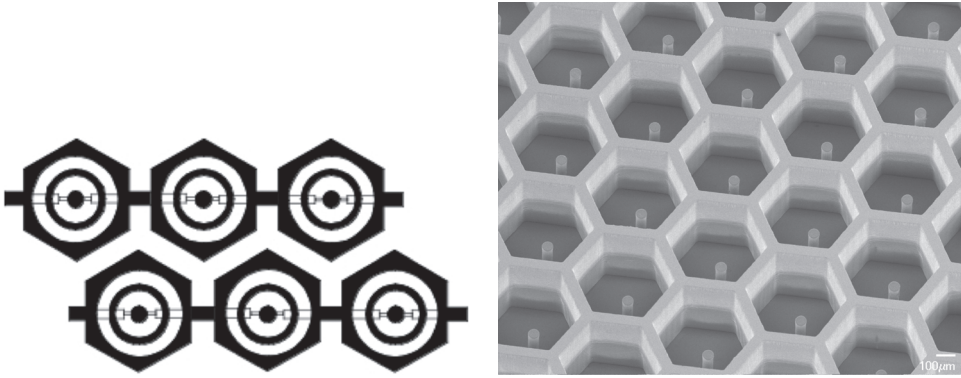


Figure 13.13 Schematics of the micro-dot, left (Biagi and Jones, 1995), by kind permission of Elsevier, and close view of the micro-pin array, right (G. Smith, personal communication).

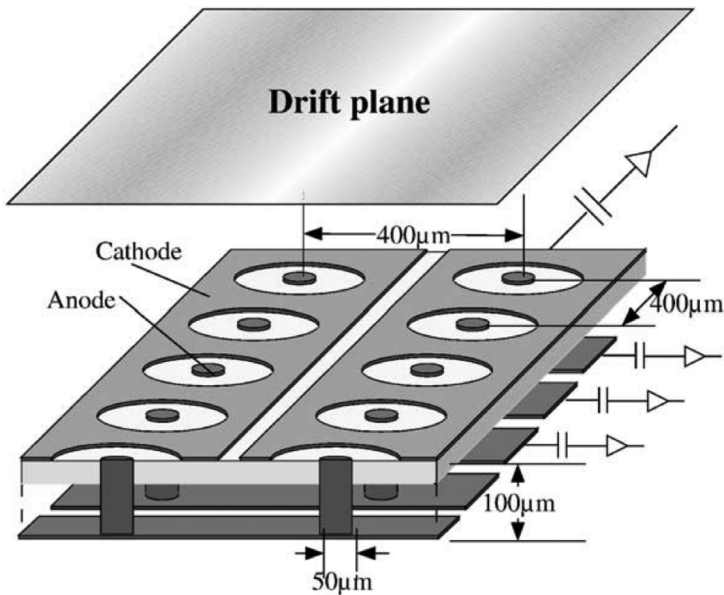


Figure 13.14 Schematics of the micro-pixel chamber (Ochi *et al.*, 2002). By kind permission of Elsevier.

individual circular anodes ensuring charge multiplication, interconnected on the back plane to provide one coordinate; a second coordinate is given by orthogonal cathode strips, as shown in the figure. While suffering, as most other MPGDs, with an initial gain shift at power on due to charging-up of the dielectric substrate, the  $\mu$ PIC chamber has been successfully used as end-plane detector for TPC readout (H. Kubo *et al.*, 2003) and time-resolved neutron imaging (Parker *et al.*, 2013).

In the second application, a selection of the detected charge and a detailed analysis of the conversion tracks permit an efficient neutron identification and localization in the presence of a gamma background.

All MPGD structures described have been tested successfully; in many cases, however, they appeared to be difficult to manufacture in reasonable sizes and quantities, and several have been discontinued.

Although not belonging to the MPGD family, the so-called ‘compteur à trous’ (CAT), shown in Figure 13.15, is an interesting addition to the field of gaseous detectors (Bartol *et al.*, 1996). Consisting of a single hole drilled through a thick printed circuit board, the counter collects and amplifies the charge released in the upper drift gap; large area devices can be implemented with a matrix of adjacent holes. Despite the expected dependence of gain from the field integral along the line of approach, the device exhibits surprisingly good energy resolution

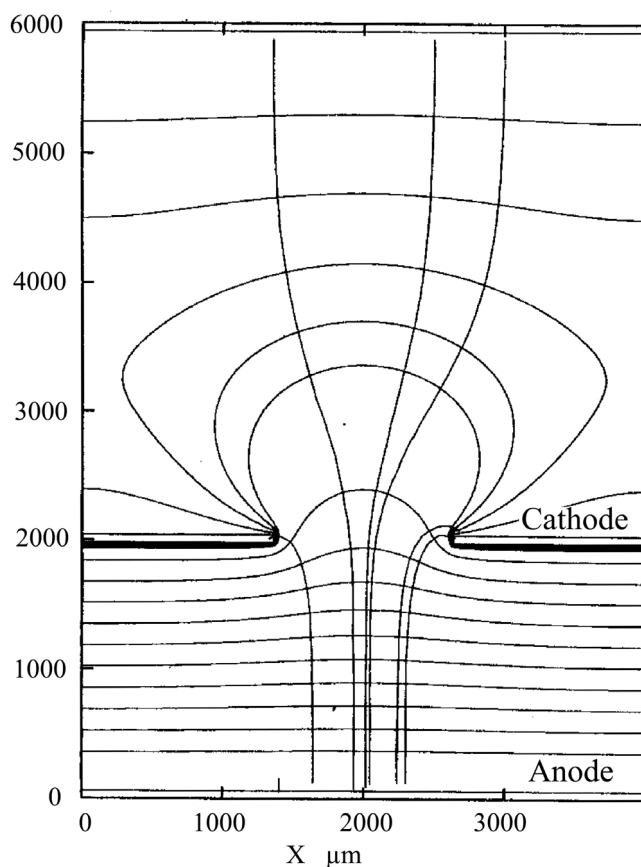


Figure 13.15 Schematics of the ‘compteur à trous’ (CAT) (Bartol *et al.*, 1996).  
By kind permission of EDP, les Editions de Physique.

(Chaplier *et al.*, 1999). Built to a reduced scale, the gas electron multiplier (GEM), described in Section 13.4, was inspired by this work.

### 13.3 Micro-mesh gaseous structure (Micromegas)

The successful development of thin-anode multi-wire and micro-strip structures sidestepped the research on gas detectors by exploiting multiplication in uniform fields. Mechanically sturdier, parallel plate counters have intrinsically better energy resolution and higher rate capability; however, the exponential dependence of gain on the gap and the sensitivity to defects causing field emission result in unstable operation and discouraged their use.

It was observed, however, that in thin, sub-mm gaps, due to saturation of the Townsend coefficient at very high fields, large gains can be attained, with a decreased sensitivity to gap variations and imperfections; this has led to the development of the micro-mesh gaseous chamber (Micromegas) (Giomataris *et al.*, 1996). The detector is built with a thin metal grid stretched at a small distance, 50 to 100  $\mu\text{m}$ , from the readout electrode; with a high field applied across the gap, typically above 30 kV/cm, electrons released in the upper drift region are collected and multiplied with large gains (Figure 13.16). To ensure the uniformity of the multiplying gap, regularly spaced insulating supports inserted during manufacturing separate anode and cathode (Figure 13.17). In the manufacturing process named bulk Micromegas, the printed circuit with readout strips constituting the anode is laminated at high temperature with an etchable polymer foil and the metal mesh; the insulator is then masked and selectively removed with a photolithographic process, producing the pillars shown in Figure 13.18 (Giomataris *et al.*, 2006).

Due to the small gap and high field, positive ions move very swiftly and induce on the anodes fast signals with only a small ion tail, the shorter the narrower the gap (Figure 13.19) (Bay *et al.*, 2002); as the overlying drift field is generally much smaller, most ions are collected on the cathode mesh, reducing the charge backflow into the drift gap.

The favourable statistical properties of charge multiplication in uniform fields, added to the reduced field dependence of gain, result in a very good energy resolution for soft X-rays, as shown in the example of Figure 13.20 (Delbart *et al.*, 2001).

Micromegas detectors can be operated with a wide choice of gases; the gain measurements shown in Figure 13.21 are an example (Bay *et al.*, 2002). The maximum gain attainable exceeds  $10^5$  making the device capable of efficiently detecting and localizing small amounts of ionization, at least in the absence of a heavily ionizing background.

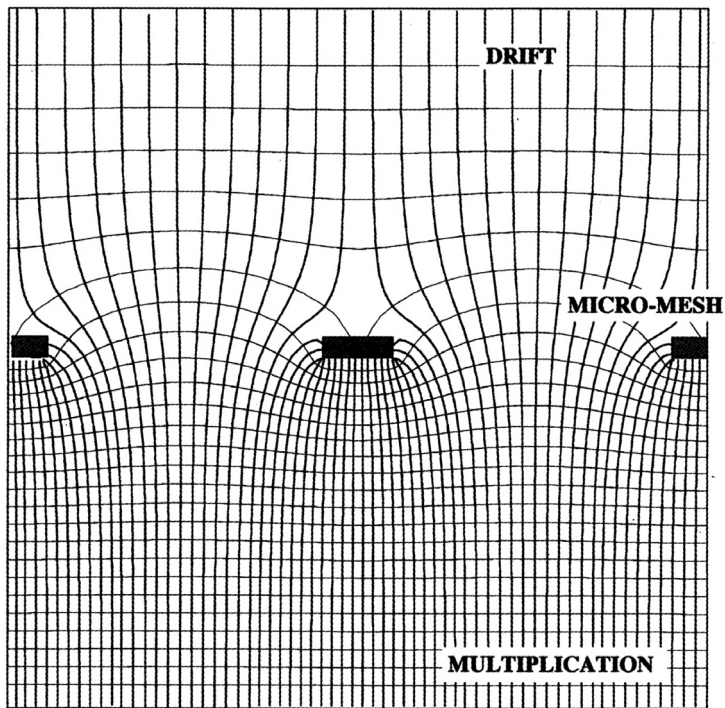


Figure 13.16 Electric field in the Micromegas (Giomataris *et al.*, 1996). By kind permission of Elsevier.

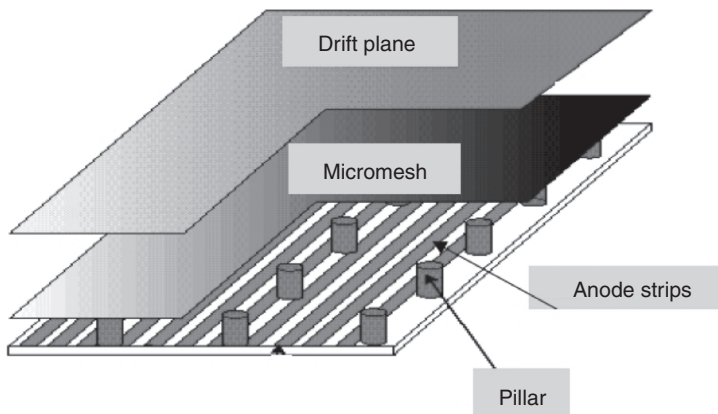


Figure 13.17 Schematics of the Micromegas construction, with insulating spacers across the multiplying gap (Giomataris *et al.*, 1996). By kind permission of Elsevier.

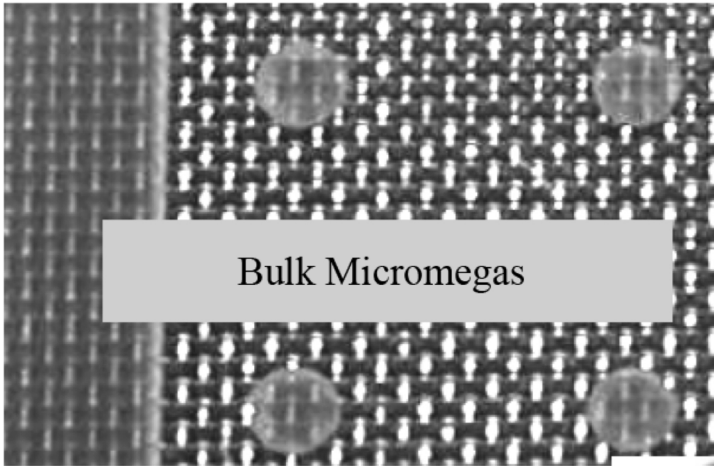


Figure 13.18 Close view of the insulating spacer pillars, 300  $\mu\text{m}$  in diameter (Giomataris *et al.*, 2006). By kind permission of Elsevier.

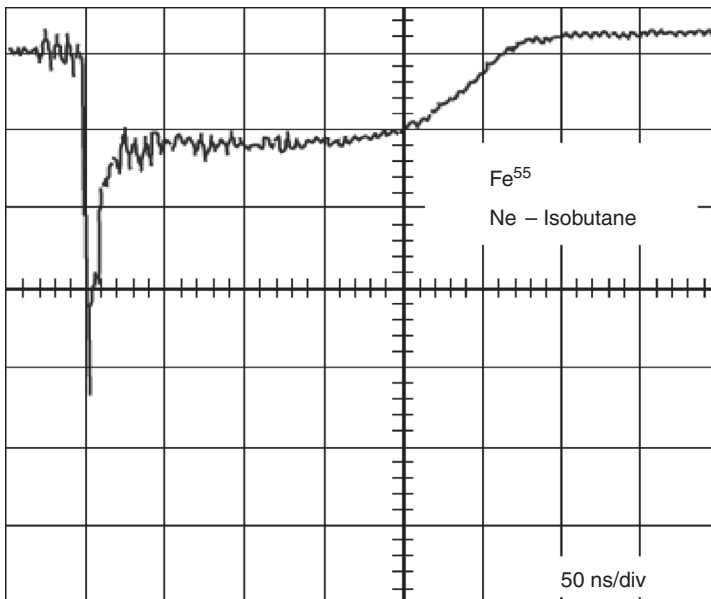


Figure 13.19 Fast signal detected on the anodes of Micromegas (Bay *et al.*, 2002). By kind permission of Elsevier.

For charged particles, a very good localization can be achieved thanks to the narrow amplification gap, small readout strip distance and the use of a low-diffusion gas. In a small system, a position accuracy of 12  $\mu\text{m}$  rms for a  $\text{CF}_4$ -isobutane filling and 100  $\mu\text{m}$  strips pitch has been obtained for fast particles

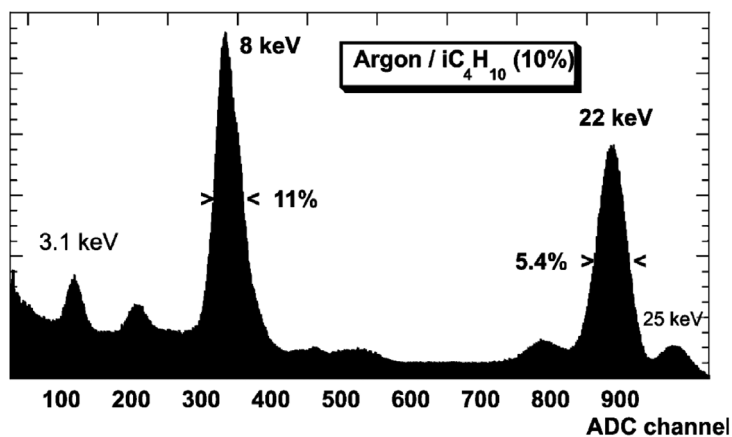


Figure 13.20 Micromegas energy resolution for a  $^{109}\text{Cd}$  source (Delbart *et al.*, 2001). By kind permission of Elsevier.

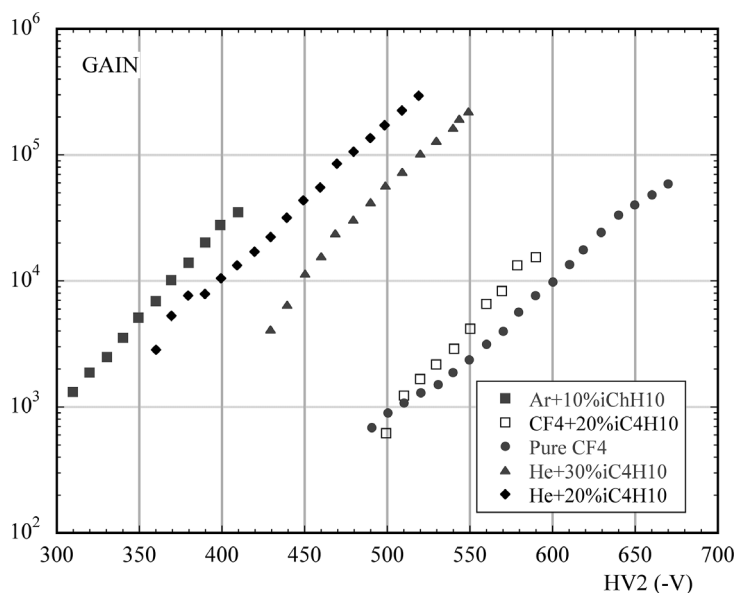


Figure 13.21 Micromegas gain as a function of voltage for several gas fillings at STP (Bay *et al.*, 2002). By kind permission of Elsevier.

perpendicular to the detector (Derré *et al.*, 2000). For larger detector sizes, practical considerations on the electronics channels density bring the space resolution to  $\sim 70\ \mu\text{m}$ , as in the Micromegas tracker for CERN's COMPASS experiment, using  $360\ \mu\text{m}$  readout strips pitch and operated with a  $\text{Ne-C}_2\text{H}_6\text{-CF}_4$  gas mixture, Figure 13.22 (Bernet *et al.*, 2005).

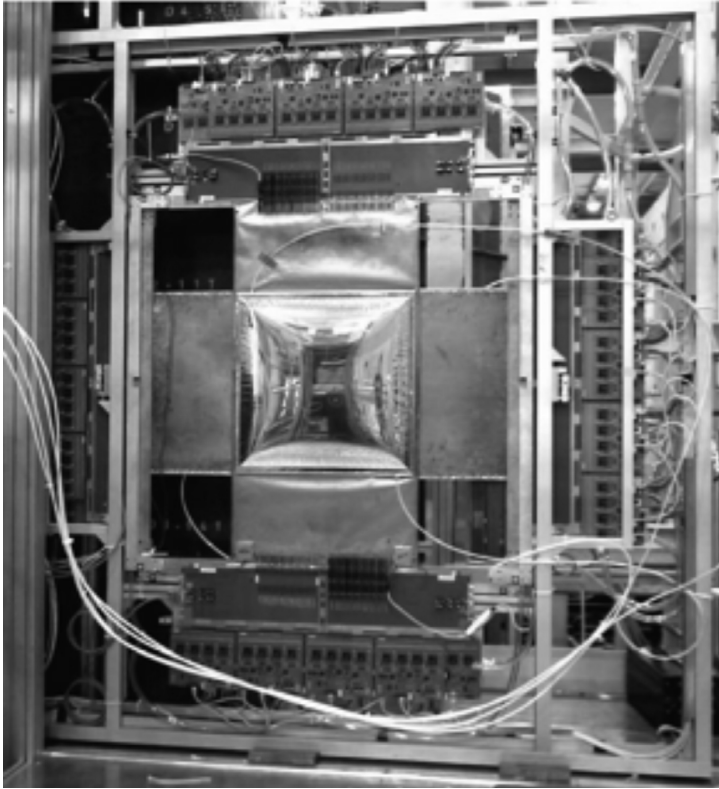


Figure 13.22 One of the Micromegas detectors in the COMPASS spectrometer, with a  $40 \times 40 \text{ cm}^2$  active area surrounded by the readout electronics (Bernet *et al.*, 2005). By kind permission of Elsevier.

As in other MPGD structures, the insurgence of discharges when the detector is exposed to a mixed field radiation limits the range of operating voltage. The sturdiness of the Micromegas electrodes prevents physical damage even in the case of repeated breakdowns, but the recovery time of the voltage supply, typically of a few ms, introduces a dead time in the operation.

Systematic studies of geometry and gas mixtures have been undertaken to try and limit the discharge probability (Bay *et al.*, 2002); Figure 13.23 is a comparison of discharge probability as a function of gain for two gas fillings, measured in a high intensity hadron beam<sup>3</sup> (Delbart *et al.*, 2002). Higher gains can be reached in helium-based mixtures, probably as a consequence of the lower ionization density of background tracks, but this is balanced by a decrease in the charge release of the tracks.

<sup>3</sup> For beam measurements, the discharge probability is normalized to the beam intensity.

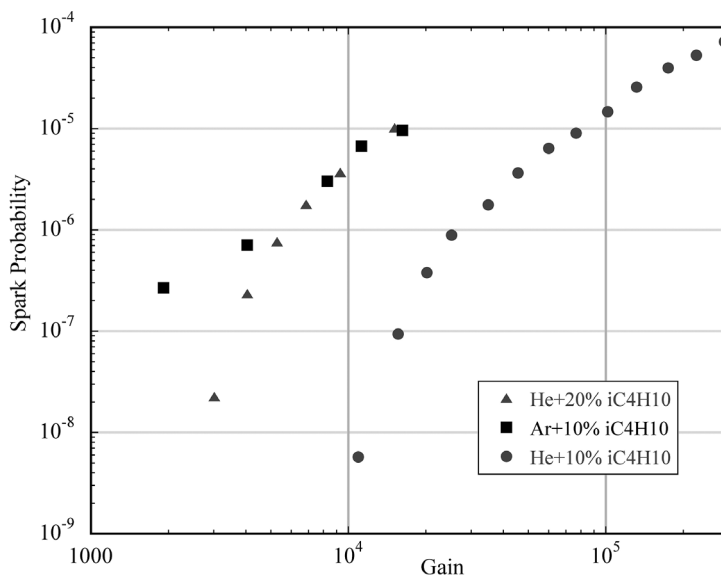


Figure 13.23 Micromegas discharge probability as a function of gain for two gas mixtures (Delbart *et al.*, 2002). By kind permission of Elsevier.

As for the MSGCs, higher gains before breakdown can be reached by adding a GEM pre-amplification stage, an advantage balanced by an increased complexity of construction of the detector (Charles *et al.*, 2011; Procureur *et al.*, 2011). Use of a high resistivity layer insulating the multiplication gap from the anode helps in dumping the discharges before full breakdown, similarly to the approach used for RPCs, see Chapter 12; this implies, however, a noticeable reduction in rate capability and can lead to gain instabilities due to charging-up (Alexopoulos *et al.*, 2011).

### 13.4 Gas electron multiplier (GEM)

The gas electron multiplier (GEM) consists of a thin, metal-clad polymer foil chemically perforated by a high density of holes, typically 100 per square mm (Sauli, 1997). Inserted between a drift and a collection electrode, with a suitable choice of the voltage on electrodes all electrons released by ionization in the overlaying gas gap drift into the holes, where charge multiplication occurs (Figure 13.24). Most of the electrons generated in the avalanches transfer into the lower region; the GEM foil acts then as a charge pre-amplifier, to a large extent preserving the original ionization pattern. Each hole acts as an independent proportional counter, screened from the neighbours; due to the high density of holes, the gain is not affected by space charge up to very high radiation fluxes.

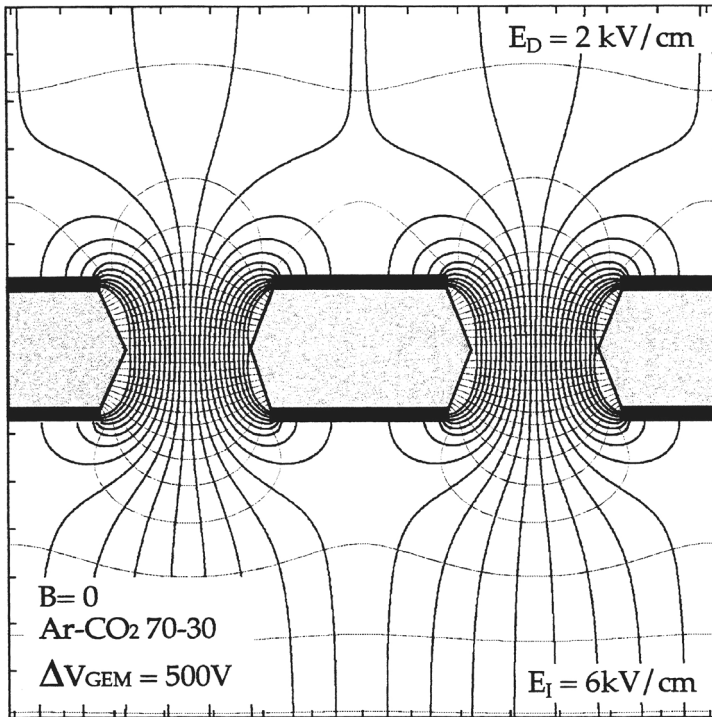


Figure 13.24 GEM electric field near the holes in typical operating conditions (Bachmann *et al.*, 1999). By kind permission of Elsevier.

As avalanche multiplication occurs almost entirely in the high dipole field within the holes, the gain is only mildly affected by external fields,<sup>4</sup> and insensitive to the foil shape, considerably relaxing the mechanical requirements. Separated from the multiplying electrode, the charge collection and readout plane can be patterned at will with strips, pads or a combination of the two.

GEM electrodes can be easily shaped to match the experimental requirements; with proper supports, they can be used to manufacture non-planar detectors. The so-called ‘standard GEM’, produced in large quantities and a wide range of shapes and size, has 70  $\mu\text{m}$  holes 140  $\mu\text{m}$  apart in a triangular pattern, etched on 50  $\mu\text{m}$  copper-clad kapton, as seen in Figure 13.25 (Altunbas *et al.*, 2002).

The GEM manufacturing method is a refinement of the double-sided printed circuit technology.<sup>5</sup> The metal-clad polymer is engraved on both sides with the desired hole pattern; a controlled immersion in a polymer-specific solvent opens the channels in the insulator. As a result of the process, the holes in the insulator tend to

<sup>4</sup> The fraction of electrons in the avalanche leaking into the lower gap and to the following electrode depends instead on the transfer field; the detected charge defines the effective gain, smaller than the total.

<sup>5</sup> Developed at CERN by Rui de Oliveira.

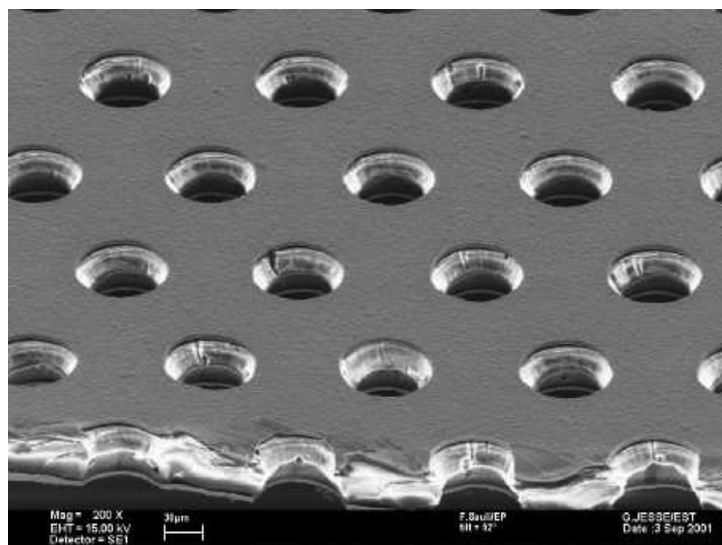


Figure 13.25 Microscope view of a GEM electrode. The holes' diameter and pitch are 70 and 140  $\mu\text{m}$ , respectively (Altunbas *et al.*, 2002). By kind permission of Elsevier.

have a double-conical shape; a thorough control of the etching conditions permits one to approach a near-cylindrical shape, demonstrated to reduce the insulator charging up and consequent gain modifications (Bachmann *et al.*, 1999). A detailed description of the manufacturing procedure is given in Walz (2010).

The described manufacturing process requires the use of two identical masks with the holes' pattern, which have to be aligned with a tolerance of a few  $\mu\text{m}$  to avoid creating slanted holes. For large areas, this becomes exceedingly difficult; a single-mask process has been developed permitting the realization of GEM foils close to a square metre (Alfonsi *et al.*, 2010; Villa *et al.*, 2011).

While the majority of GEM-based detectors have a rectangular geometry, the electrode geometry can be shaped according to the experimental needs; Figure 13.26 is an example of an electrode developed for the forward tracker of the TOTEM experiment at CERN (Lami *et al.*, 2006; Antchev *et al.*, 2010).

Alternative manufacturing methods making use of mechanical or laser drilling of thicker supports, generally with a coarser holes' pitch, have been developed for applications requiring moderate localization accuracies (Periale *et al.*, 2002; Chechik *et al.*, 2004; Badertscher *et al.*, 2010); they are generally referred to as thick GEM (THGEM). Figure 13.27 shows a large THGEM electrode, developed for the COMPASS RICH upgrade, having 400  $\mu\text{m}$  diameter holes on a 600  $\mu\text{m}$  thick printed circuit board (Alexeev *et al.*, 2010). For a review see Breskin *et al.* (2009).

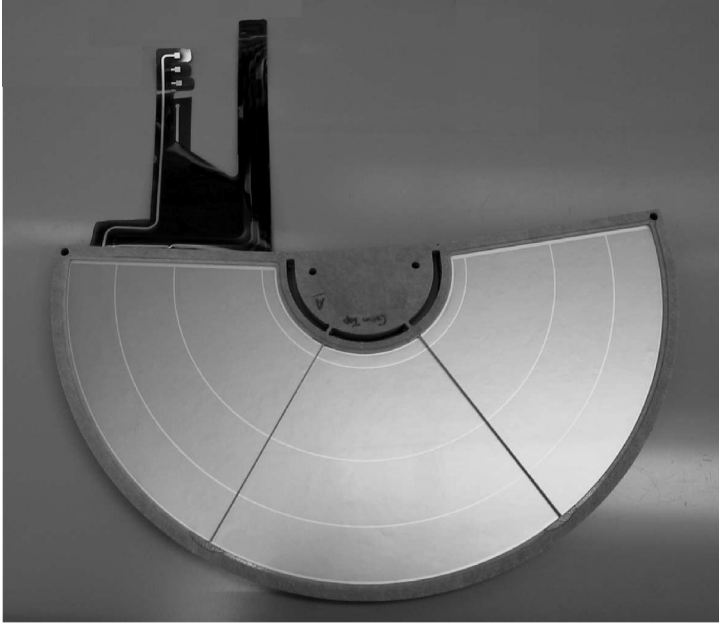


Figure 13.26 A semi-circular GEM electrode, 30 cm in diameter, for the TOTEM experiment. Picture CERN (2004).



Figure 13.27 A prototype thick-GEM electrode developed for the COMPASS RICH upgrade (Alexeev *et al.*, 2010). By kind permission of Elsevier.

GEM-based detectors have been tested in a variety of gas fillings and operating conditions, including low and high pressures; for a comprehensive review see Sauli (2014). Gains above one thousand can be reached in the detection of fast charged particles and soft X-rays; in the presence of heavily ionizing tracks, however, the discharge probability is comparable to the one observed in other micro-pattern devices, confirming the fundamental nature of the Raether limit (Bressan *et al.*, 1999a).

A unique feature of the GEM concept is that several amplifiers can be cascaded within the same detector, separated by low field transfer gaps (Bouclier *et al.*, 1997; Büttner *et al.*, 1998; Bressan *et al.*, 1999b). The overall gain of a multiple structure corresponds to the product of the gains of each element, once the transfer efficiency is taken into account (the so-called effective gain); as shown in Figure 13.28 for a double-GEM detector, operated with an argon-CO<sub>2</sub> gas mixture, high gains can be obtained with each element at a much lower voltage than for a single device, largely improving the reliability of the detector (Bachmann *et al.*, 1999). Extensive tests demonstrate that a cascade of three electrodes, named triple-GEM (Figure 13.29) guarantees the reliability and breakdown suppression needed in harsh beam conditions (Ziegler *et al.*, 2001; Ketzner *et al.*, 2004); the required potentials can be applied to the electrodes through simple resistor chains or dedicated power supply systems.

Measurements of discharge probability on exposure to a heavily ionizing background demonstrate that in multiple structures discharges occur at higher

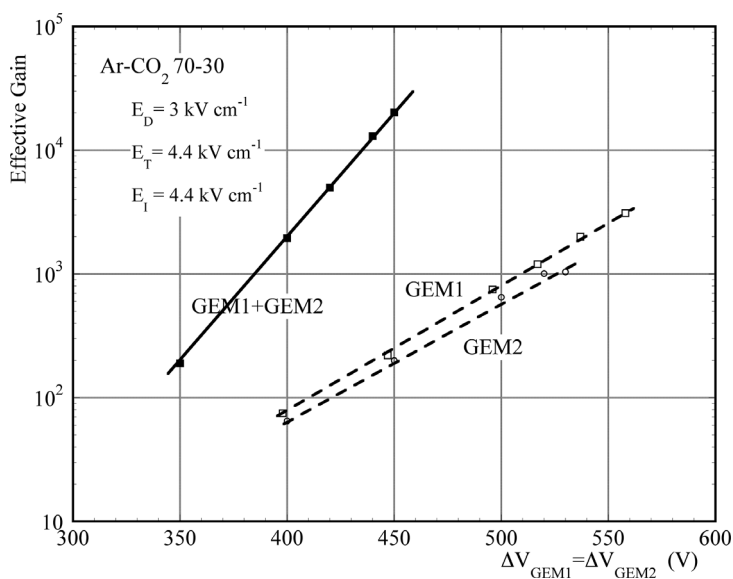


Figure 13.28 Effective gains of two single GEM electrodes, and combined gain of a double structure (Bachmann *et al.*, 1999). By kind permission of Elsevier.

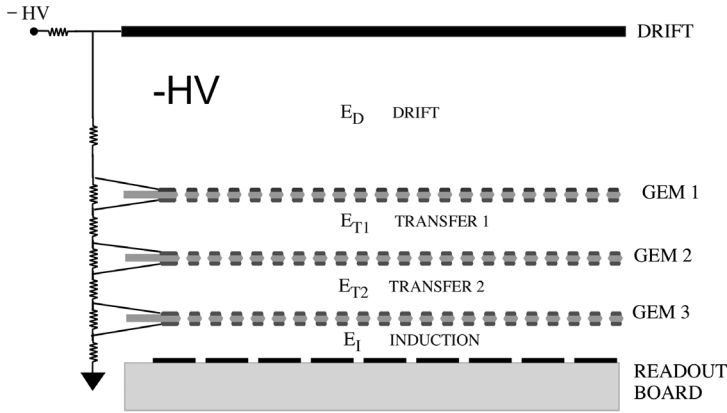


Figure 13.29 Schematics of a triple-GEM chamber and resistor chain used to distribute the voltage to the electrodes (Ketzer *et al.*, 2004). By kind permission of Elsevier.

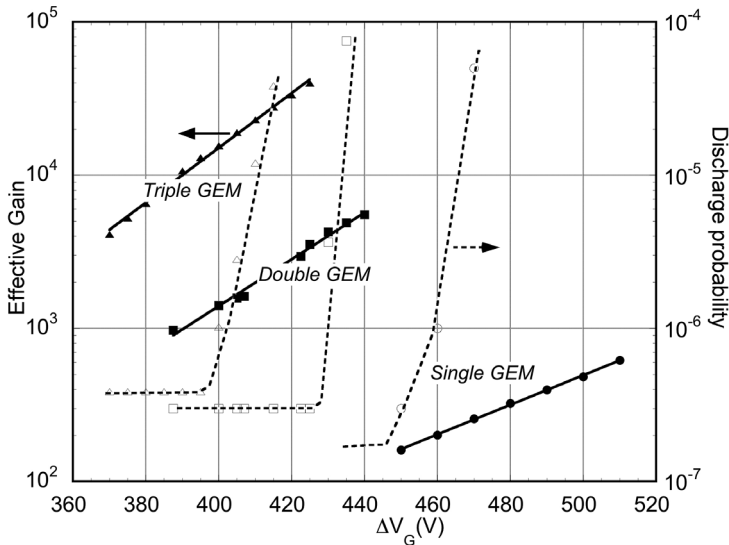


Figure 13.30 Gain (full lines) and discharge probability (dashed curves) of single, double and triple-GEM detectors as a function of the individual GEM voltages (Bachmann *et al.*, 2002). By kind permission of Elsevier.

gains, as shown in Figure 13.30 (Bachmann *et al.*, 2002); the horizontal scale is the voltage applied to each GEM electrode. For a triple-GEM device, the onset of discharge is at a gain of  $\sim 3 \times 10^4$ , comfortably above the one needed to detect fast particles. Since the average ionization charge of the  $\alpha$  particles used for the measurement is around 5000 (see Section 13.1) this seems to violate the Raether

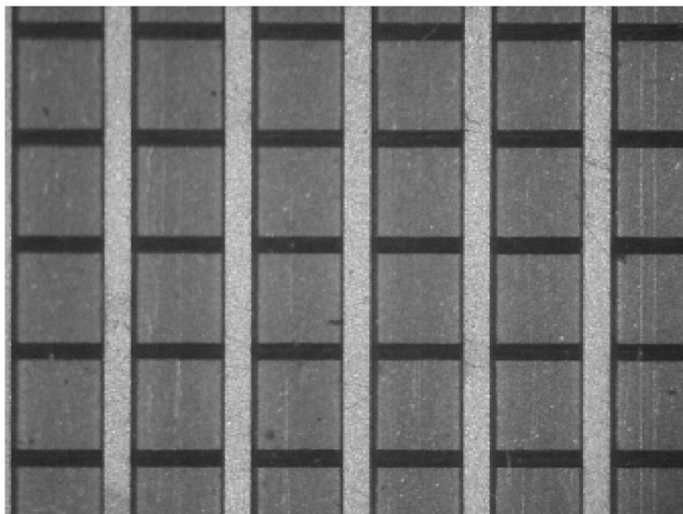


Figure 13.31 Two-dimensional readout circuit with strips at 400 pitch (Bressan *et al.*, 1999c). By kind permission of Elsevier.

limit, but is probably a consequence of the added lateral electron diffusion in the cascaded structures, spreading the avalanche charge into many multiplying holes, kept below the discharge limit in each hole.

Separated from the multiplying elements, the signal collection electrode can be patterned with strips or pads of arbitrary shape. A circuit widely used for two-dimensional projective readout is shown in Figure 13.31; realized on a 50  $\mu\text{m}$  polymer foil with the same technology used for GEM manufacturing, it has 80  $\mu\text{m}$  wide strips on the side facing the multiplier and, insulated from them, wider strips on the lower coordinate, to ensure equal sharing of the collected charge along the two directions (Bressan *et al.*, 1999c). The circuit can be realized with individual readout pads in the part of the detector exposed to higher radiation flux, and projective strips to cover the remaining area (Krämer *et al.*, 2008).

Depending on the experimental needs, the detectors can be operated with a wide choice of gas fillings; Figure 13.32 gives examples of effective gain measured with a triple-GEM detector in several gas mixtures (Breskin *et al.*, 2002). Very high gains can be reached in pure carbon tetrafluoride, permitting the detection of single photoelectrons as for Cherenkov ring imaging applications (see Chapter 14).

With non-flammable argon-CO<sub>2</sub> mixtures, GEM chambers provide routinely for fast particles detection efficiencies close to 100%, localization accuracies around 70  $\mu\text{m}$  rms and 10 ns resolution (Ketzner *et al.*, 2004). Use of a faster gas mixture containing CF<sub>4</sub> permits one to achieve a time resolution better than 5 ns rms, an essential advantage when operating around fast cycling colliders (Alfonsi *et al.*, 2004).

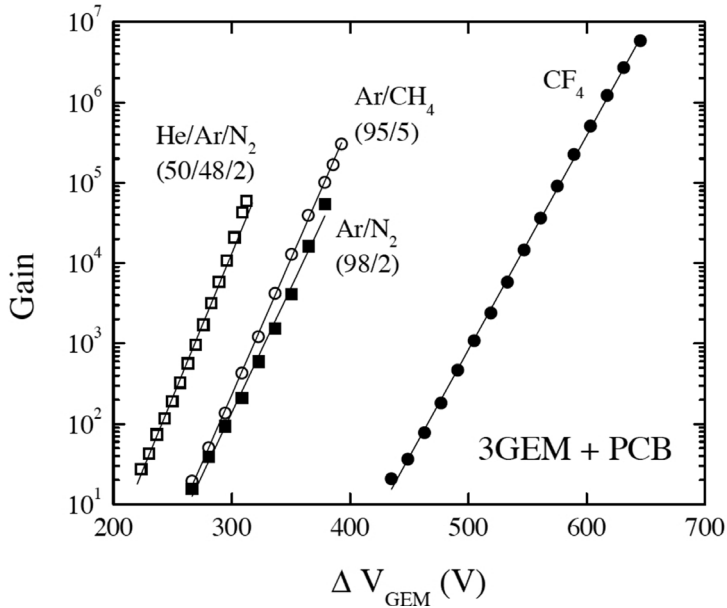


Figure 13.32 Triple-GEM gain as a function of voltage in several gases (Breskin *et al.*, 2002). By kind permission of Elsevier.

A set of medium size ( $30 \times 30 \text{ cm}^2$  active) triple-GEM chambers with projective cartesian coordinates readout has been used for many years in the harsh running conditions of the COMPASS spectrometer at CERN. One of the detectors, instrumented by a high-density charge-recording readout electronics, is shown in Figure 13.33 (Altunbas *et al.*, 2002; Ketzer *et al.*, 2004). The TOTEM detector at CERN, shown in Figure 13.34, deploys two sets of triple-GEM chambers built with the semi-circular elements shown in Figure 13.26 (Bagliesi *et al.*, 2010).

GEM detector foils can be assembled in non-planar geometry with the use of appropriate edge supports; Figure 13.35 is a cylindrical triple-GEM detector in construction for the KLOE-2 inner tracker at the Italian Laboratori Nazionali di Frascati (LNF) (Bencivenni and Domenici, 2007; Balla *et al.*, 2011).

Owing to the absence of thin anodes, GEM detectors have a very high rate capability; on exposure to a soft X-ray generator, the gain remains constant up to and above a flux of  $1 \text{ MHz mm}^{-2}$ , as shown in Figure 13.36, measured with a single GEM chamber operated at a gain around  $10^3$  (Benlloch *et al.*, 1998).

Thanks to the absence of thin anodes, GEM detectors are insensitive to radiation damage induced by polymerization, up to very high integrated fluxes, as discussed in Section 16.5.

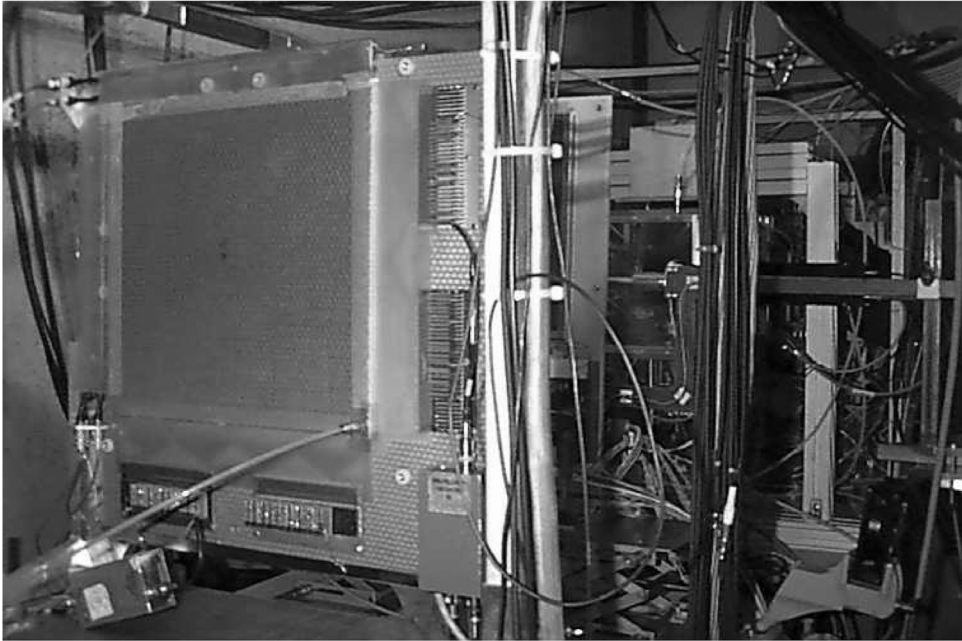


Figure 13.33 One of the triple-GEM detectors installed in the COMPASS spectrometer at CERN (Ketzer *et al.*, 2004). By kind permission of Elsevier.

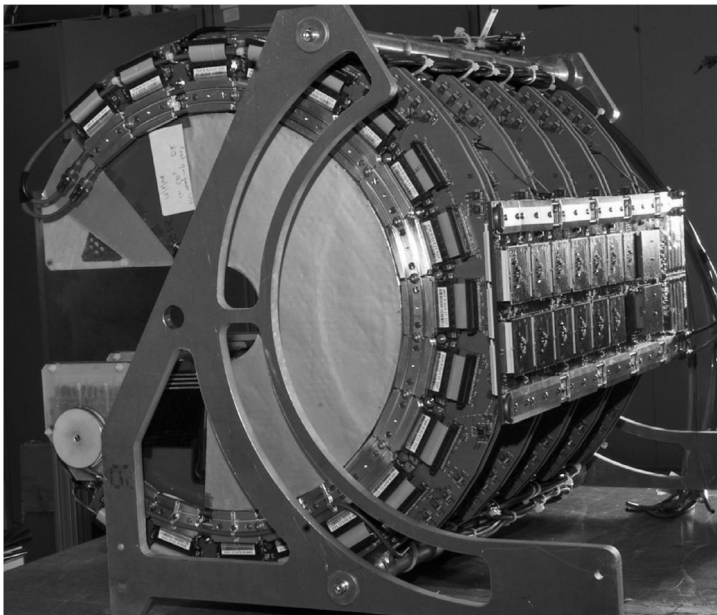


Figure 13.34 A module of the TOTEM tracker, assembly of five triple-GEM detectors. A symmetric segment closes in from the left and completes the detector (Bagliesi *et al.*, 2010). By kind permission of Elsevier.

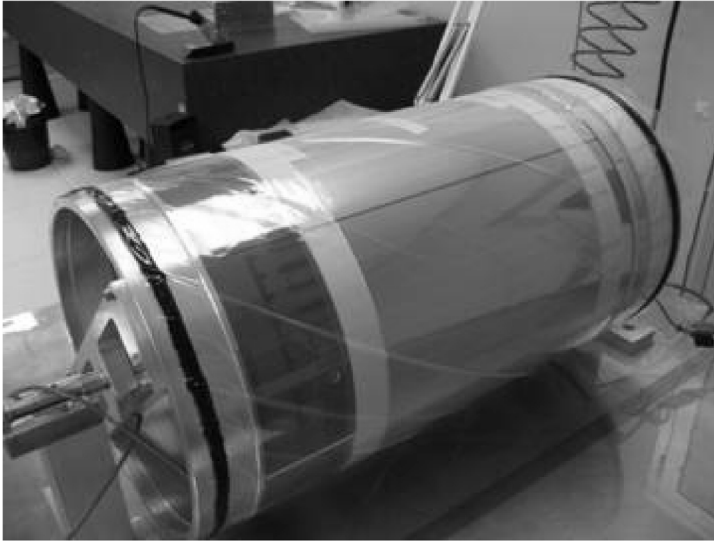


Figure 13.35 Prototype cylindrical GEM detector for KLOE-2 (Bencivenni and Domenici, 2007). By kind permission of Elsevier.

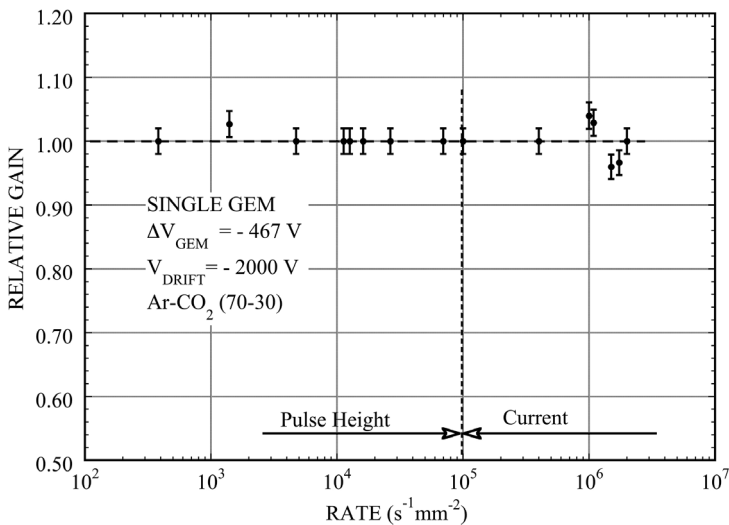


Figure 13.36 Normalized gain of a single GEM detector as a function of rate (Benlloch *et al.*, 1998). By kind permission of Elsevier.

### 13.5 MPGD readout of time projection chambers

Used for time projection chambers end-cap readout, MPGDs have many advantages compared to the standard MWPC: simpler and more robust construction, better space and multi-track resolution, absence of distortions due to non-parallel

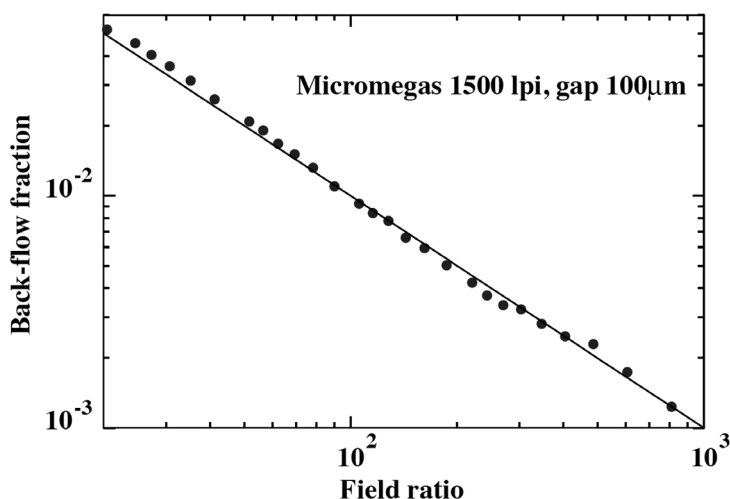


Figure 13.37 Positive ion backflow in Micromegas as a function of the ratio of multiplication and drift fields (Colas, 2004). By kind permission of Elsevier.

electric and magnetic fields close to the anode wires, and a substantial reduction of the positive ion backflow into the drift volume, thanks to their electric field structure. With Micromegas, using a narrow pitch cathode mesh and a gas filling chosen to enhance the transverse spread of the avalanches, the ion feedback is simply equal to the ratio between the drift and multiplying fields, typically around 1%, see Figure 13.37 (Colas, 2004).<sup>6</sup> With a thorough adjustment of the various fields in a multi-GEM structure, the backflow can be reduced below 1% (Bondar *et al.*, 2003); in the presence of a longitudinal magnetic field, due to the different effects of diffusion on ions and electrons, this ratio is further decreased below a few parts in a thousand, Figure 13.38 (Killenberg *et al.*, 2004).

A system of large volume TPC detectors with MPGD readout operates in the T2K neutrino experiment at KEK surrounding the active target. Each TPC module is instrumented with a matrix of Micromegas modules with pads readout, and records the pattern and differential energy loss of charged particles resulting from the interaction of neutrinos in the target (Abgrall *et al.*, 2011). Fundamental to the particle identification power of the detector, a calibration procedure and ambient parameter control ensures a uniformity of energy loss measurement better than 3% over the whole detector area (Delbart, 2010).

<sup>6</sup> The fractional ion backflow is defined as the ratio of the ion's current reaching the drift electrode to the electron current collected at the anodes.

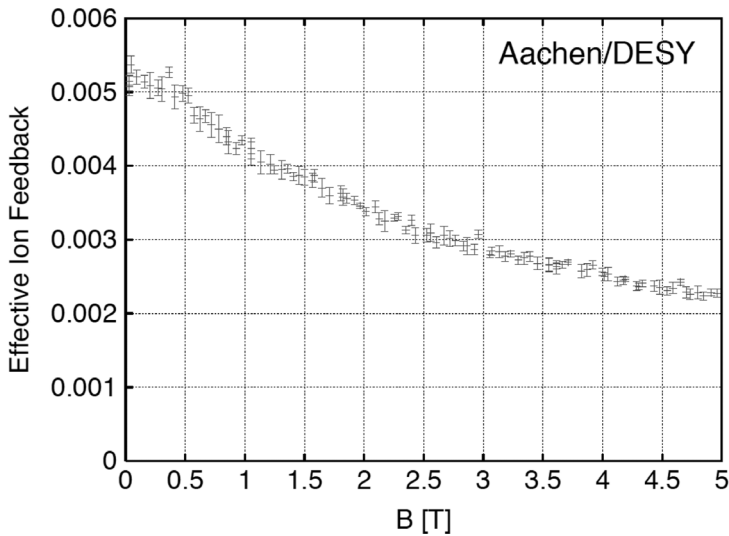


Figure 13.38 Fractional ions backflow in a TPC with GEM readout as a function of magnetic field (Killenberg *et al.*, 2004). By kind permission of Elsevier.

MPGD end-cap systems for TPCs have been the subject of many studies, aiming at optimizing the signal pads shape and reducing the number of readout channels needed (Kaminski *et al.*, 2006; Ledermann *et al.*, 2007; Oda *et al.*, 2006). A way to preserve and even improve the localization properties of detectors, while reducing the number of readout channels, has been devised using a resistive foil between the last multiplication stage and the signal readout electrode (Dixit *et al.*, 2004; Boudjemline *et al.*, 2007). With careful adjustment of the parameters, the collected charge is spread over a larger area, reducing the required density of readout channels. A possible drawback of the method is a reduced rate capability, due to the longer signal integration times.

The choice of the operating gas in TPC-like detectors is dictated by several requirements: reasonably high drift velocities at moderate electric fields, low electron diffusion and non-flammability. In the framework of the study of detectors for the International Linear Collider (ILC), a good compromise has been found with the so-called TDR gas mixture (Ar-CH<sub>4</sub>-CO<sub>2</sub> in the volume proportions 93–5–2). Figure 13.39 shows measured values of transverse space resolution as a function of drift distance and magnetic field, for two choices of the readout pads geometry (Janssen *et al.*, 2006).

Mixtures containing carbon tetrafluoride provide even better space resolution, thanks to the lower diffusion, with the disadvantage of requiring higher operating voltages (Oda *et al.*, 2006; Kobayashi *et al.*, 2011).

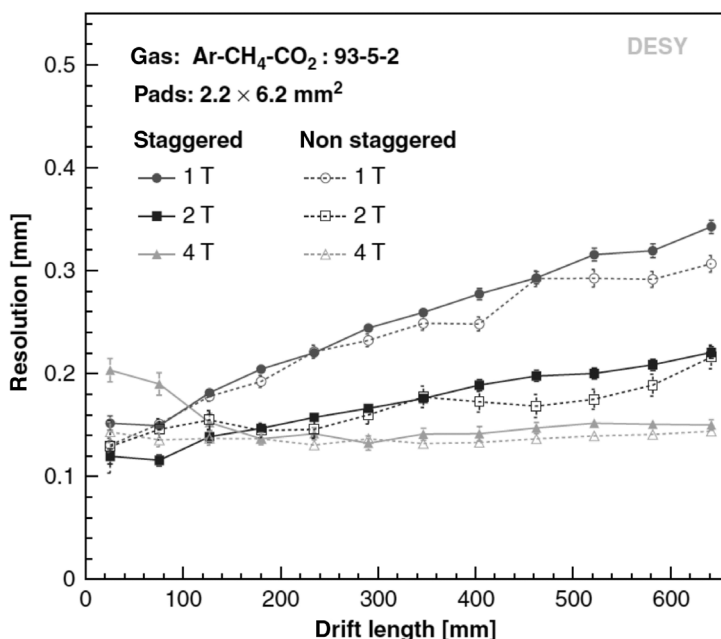


Figure 13.39 Transverse resolution of a TPC with GEM readout as a function of drift distance for several values of magnetic field and two readout pads geometries (Janssen *et al.*, 2006). By kind permission of Elsevier.

### 13.6 Active pixel readout

The use of anode pad arrays for the signal readout permits one to exploit at best the intrinsic high-granularity properties of MPGDs. The use of conventional systems of external front-end electronics becomes, however, very impractical for small pixel sizes; this has suggested the use of solid-state active pixel electronic circuits for direct collection and recording of the charge generated in the gaseous multiplication process.

In the X-ray polarimeter, a detector developed for astrophysics imaging applications, a custom-made CMOS integrated circuit with  $\sim 2000$  pixels at  $80 \mu\text{m}$  pitch collects the ionization released in the gas, after amplification with a GEM electrode (Bellazzini *et al.*, 2004). Figure 13.40 is an example of the two-dimensional recording of the ionization trail of a  $5.2 \text{ keV}$  photoelectron released by soft X-rays interacting in the gas (Bellazzini *et al.*, 2007a); the inset gives the size of the image. Analysis of the differential charge deposition along the track, represented in the figure by the size of the pixels, permits one to identify the higher energy loss at the track's end, and therefore the point and direction of emission, providing information on the X-ray polarization.

Thanks to the very low input capacitance and an electronic noise (typically around 50 electrons rms), even at moderate proportional gains the detector can

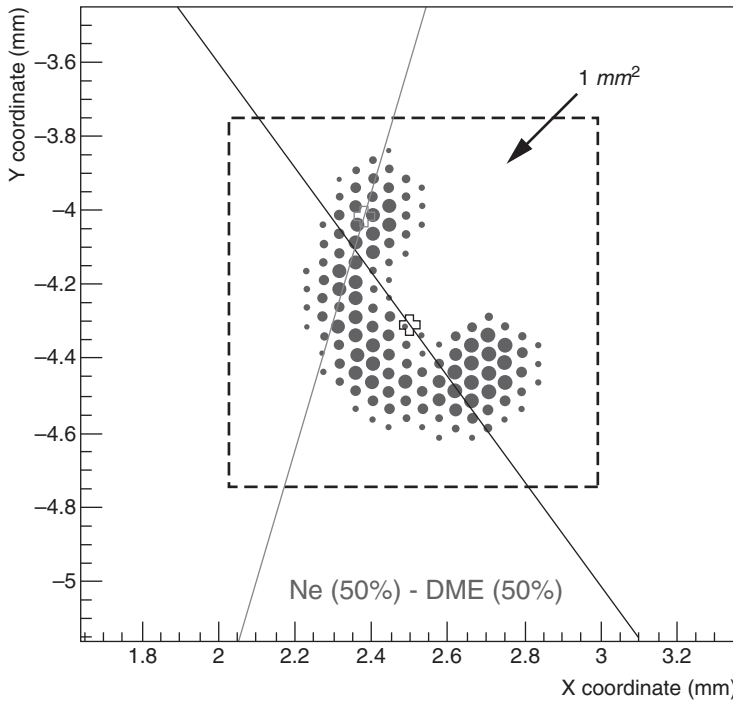


Figure 13.40 A 5.2 keV photoelectron track recorded with the GEM polarimeter (Bellazzini *et al.*, 2007a). By kind permission of Elsevier.

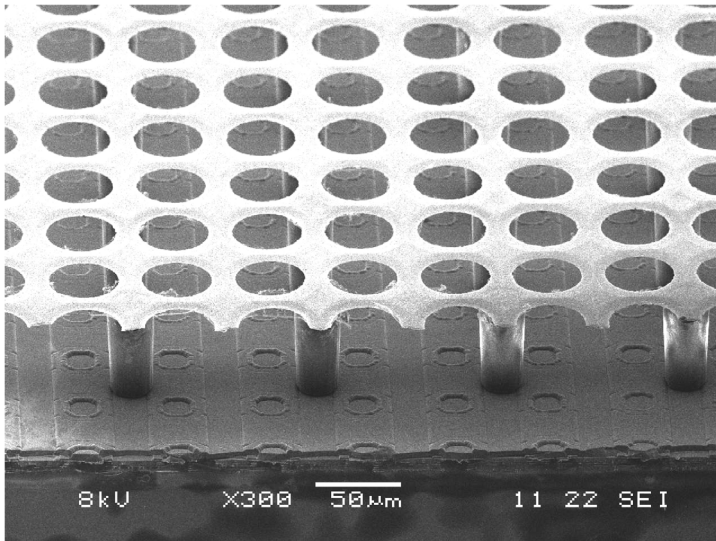


Figure 13.41 The GridPix detector, integrating a Micromegas-like structure over a solid-state pixel readout chip (van der Graaf, 2007). By kind permission of Elsevier.

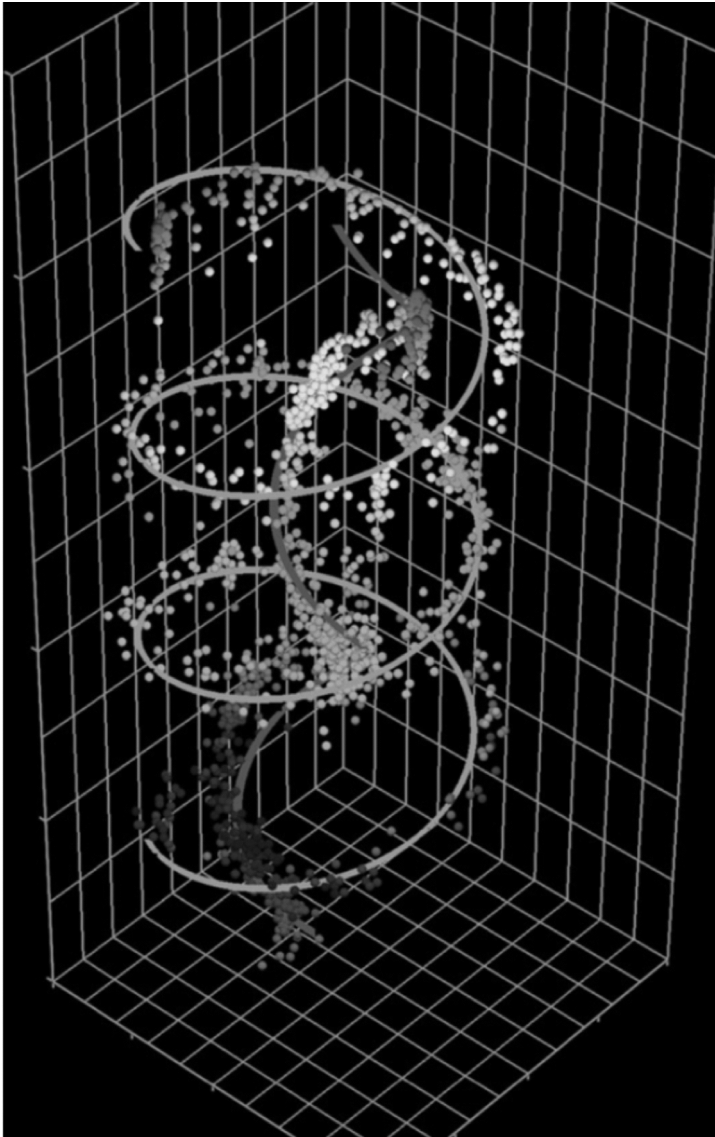


Figure 13.42 Low-energy electron tracks spiralling in a magnetic field, detected by a GridPix detector with TimePix readout (van der Graaf, 2011). By kind permission of Elsevier.

achieve single electron sensitivity and can be used for UV photon imaging (Bellazzini *et al.*, 2007b).

The active gaseous device can be directly built over an existing solid-state pixel circuit using silicon wafer post-processing technologies (Chefdeville *et al.*, 2006). Named InGrid or GridPix, these detectors combine the Medipix (Llopart *et al.*, 2002) or Timepix (Llopart *et al.*, 2007) CMOS pixel readout chips,

developed for medical imaging using solid state sensors, with a Micromegas or GEM structure directly built over the solid state sensor (Figure 13.41) (van der Graaf, 2007; Malai *et al.*, 2011). Combined with a drift space in a TPC-like structure, GridPix detectors are capable of imaging sub-mm ionization trails, recording individual ionization clusters, as shown by the example in Figure 13.42 (van der Graaf, 2011).

A drawback of the described approach is the possible damage to the sensitive electronics caused by gas discharges. Various methods of spark protection have been developed, coating the silicon chip with insulating or high-resistivity layers (Bilevych *et al.*, 2011; van der Graaf, 2011).

### 13.7 MPGD applications

While the main motivation for the development of the new generations of micro-pattern devices has been particle tracking in high-energy physics, many other applications have been developed by exploiting the performances of the detectors. Only a short summary is given here; for detailed reviews see Titov (2007); Titov (2012); Sauli (2014):

- High rate imaging of soft X-rays for plasma diagnostics (Pacella *et al.*, 2001; Pacella *et al.*, 2003);
- X- and  $\gamma$ -ray astronomy and polarimetry (Bellazzini *et al.*, 2002; Black *et al.*, 2003; Bellazzini and Muleri, 2010; Bernard and Delbart, 2012);
- High rate  $\gamma$ -ray imaging for medical portal imaging (Östling *et al.*, 2000; Östling *et al.*, 2003);
- UV and visible-range gaseous photomultipliers (Buzulutskov *et al.*, 2000; Breskin *et al.*, 2001; Mörmann *et al.*, 2003; Breskin *et al.*, 2010).

The detection and imaging of UV photons for Cherenkov ring imaging are covered in the next chapter.

#### Further reading

- Sauli, F. and Sharma, A. (1999) Micropattern Gaseous Detectors. *Ann. Rev. Nucl. Part. Sci.* **49**, 341.
- Titov, M. (2007) New developments and future perspectives of gaseous detectors. *Nucl. Instr. And Meth.* **A581**, 25.
- Sauli, F. (2013) Gas Electron Multiplier (GEM) detectors: principles of operation and applications, in *Comprehensive Biomedical Physics Vol. 6*, M. Danielsson (ed.) (Elsevier).

#### Selected conference proceedings

- MPGD2011 (2013) Second International Conference on Micro-Pattern Gaseous Detectors, *JINST* **8**.